**Phenol transformation photosensitised by quinoid compounds**

# UNIVERSITÀ DEGLI STUDI DI TORINO



V. Maurino, A. Bedini, D. Borghesi, D. Vione, C. Minero. Phenol Transformation Photosensitised by Quinoid Compounds. *Phys. Chem. Chem. Phys.* **2011**, *13*, 11213-11221.
DOI: 10.1039/c1cp20355j

# PHENOL TRANSFORMATION PHOTOSENSITISED BY QUINOID COMPOUNDS

**Valter Maurino,[a] Andrea Bedini,[a] Daniele Borghesi,[a] Davide Vione,[a,b,]* Claudio Minero[a,]***

The phototransformation of phenol in aqueous solution was studied with different quinoid compounds, which are usually detected on atmospheric particulate matter: 2-ethylanthraquinone (EtAQ), benzanthracene-7,12-dione (BAD), 5,12-naphthacenequinone (NQ), 9,10-anthraquinone (AQ), and 2,6-dihydroxyanthraquinone (DAQ). All the studied quinones were able to sensitise the phototransformation of phenol. Under blue-light irradiation the approximated, polychromatic quantum yields for phenol photodegradation were in the order AQ > BAD > EtAQ > NQ > DAQ. Quantum mechanical calculations showed that AQ and DAQ have a very different spin distribution in the triplet state (largely located on the carbonyl oxygen and delocalised over the aromatic ring, respectively) that could account for the difference in reactivity. The spin distribution of EtAQ is similar to that of AQ. Under simulated sunlight, EtAQ induced the highest rate of phenol degradation. Radiation-excited EtAQ would oxidise both ground-state EtAQ and phenol; a kinetic model that excludes the $^{\bullet}OH$ radical and singlet oxygen as reactive species is supported by the experimental data. Quinones were also able to oxidise nitrite to nitrogen dioxide, thereby inducing phenol nitration. Such a process is a potential source of nitrogen dioxide and nitrophenols in the atmospheric aerosols.

## Introduction

Photochemical processes that take place on the surface of atmospheric particulate matter are potentially important pathways for the transformation of organic and inorganic compounds, for the generation of reactive species and for the production of oligomers such as the humic-like substances.[1-3] Such processes include direct photolysis of sunlight-absorbing molecules, transformations sensitised by photoactive compounds via singlet oxygen or the excited triplet states, and reactions with atmospheric oxidants and photogenerated radical species (e.g. $^{\bullet}OH$, $^{\bullet}NO_2$, $Cl_2^{-\bullet}$, $Br_2^{-\bullet}$).[4] Atmospheric photosensitisers, among which are aromatic carbonyls, quinones and furans, can enhance the phototransformation of other organic molecules.[5,6] The transformation process involves absorption of sunlight by the photosensitiser P, with electron transition from the ground to the first singlet state ($P^{S1}$), followed by deactivation back to the ground state or by inter-system crossing (ISC) to the first triplet state ($P^{T1}$). The triplet state could undergo deactivation, react with ground-state molecular oxygen ($^3O_2$) to yield singlet oxygen ($^1O_2$), or react with an oxidisable substrate S via energy, electron or hydrogen transfer.[7,8]

$$P + h\nu \rightarrow P^{S1} \quad (1)$$
$$P^{S1} \rightarrow P \quad (2)$$
$$P^{S1} \text{—(ISC)}\rightarrow P^{T1} \quad (3)$$
$$P^{T1} \rightarrow P \quad (4)$$
$$P^{T1} + {}^3O_2 \rightarrow P + {}^1O_2 \quad (5)$$
$${}^1O_2 + S \rightarrow \text{products} \quad (6)$$
$$P^{T1} + S \rightarrow \text{products} \quad (7)$$

Quinoid compounds are common components of atmospheric particulate matter, where they mainly occur as primary or secondary pollutants.[9] Figure ESI1 shows the oxygenated aromatic compounds, including the quinones, detected on atmospheric particulate matter next to a high-traffic road near the town of Torino (NW Italy).[10] Primary emission sources of these compounds to the atmosphere are traffic,[11] industrial activities [12] and house heating.[13] Quinones can also be formed as secondary pollutants upon atmospheric oxidation of polycyclic aromatic hydrocarbons (PAHs), in the presence of reactive species such as $^{\bullet}OH$ and $^{\bullet}NO_3$.[14]

Atmospheric quinones are generally able to absorb sunlight,[15,16] which induces a singlet-singlet transition (n-π* or π-π*) that can be followed by inter-system crossing to the first triplet state, responsible for the photochemical activity.[17,18] Photoinduced reactions could be intra- or inter-molecular electron transfer, hydrogen abstraction and cycloaddition.[19-21]

The majority of previous studies of quinone reactivity have been carried out in organic solvents or in water-acetonitrile mixtures, but it has been demonstrated that quinones can also act as photosensitisers in aqueous solution.[22] In a study of the transformation of phenolic compounds, photosensitised by the water-soluble anthraquinone-2-sulphonate we have detected potential secondary pollutants such as byphenyls and dibenzofurans, which were formed by dimerisation of phenol.[23]

The present study is focused on phenol phototransformation processes sensitised by quinones that are actually found on atmospheric particulate matter: 2-ethylanthraquinone (EtAQ), benzanthracene-7,12-dione (BAD), 5,12-naphthacenequinone (NQ), 9,10-anthraquinone (AQ), and 2,6-dihydroxyanthraquinone (DAQ).[8,10] The structures of the investigated compounds (and of the detected transformation intermediates, *vide infra*) are reproduced in Scheme ESI2. Phenol was chosen as substrate because of its atmospheric occurrence as a transformation intermediate of benzene.[24]

The ability of the studied quinones to induce the nitration of phenol in the presence of nitrite under irradiation was also investigated. Indeed, nitration and photonitration processes of phenolic compounds are important pathways that yield highly phytotoxic nitrophenols in the atmosphere. Such compounds are strongly suspected to substantially contribute to forest damage in polluted areas and in their downwind regions.[25] A combination of field,[26] laboratory [27] and modelling data [28] suggests that aqueous-phase nitration and photonitration can play a substantial role in the occurrence of nitrated phenols in the atmosphere.

## Experimental

### Reagents and materials

2-Ethylanthraquinone (EtAQ), benzanthracene-7,12-dione (BAD), 5,12-naphthacenequinone (NQ), 9,10-anthraquinone (AQ), 2,6-dihydroxyanthraquinone (DAQ) (all purity grade ≥ 97%), phenol, catechol, 4-phenoxyphenol, 2,2'-dihydroxybiphenyl, 4,4'-dihydroxybiphenyl (all purity grade ≥ 99%), 4-aminoantipyrine (98%), $Na_2SO_4$ (> 99.5%), $H_2SO_4$ (95-97%) and horseradish peroxidase were purchased from Aldrich, $H_2O_2$ (35%) from VWR Int. Acetonitrile was LiChrosolv gradient grade and dichloromethane Suprasolv grade from VWR Int. All reagents were used as received, without further purification. The quinones under study were supported on hollow glass spheres (9-13 μm average diameter) from Aldrich.

### Quinone deposition on glass spheres

The studied quinones were not sufficiently soluble in water to enable irradiation in solution. They were thus deposited on glass spheres that would also simulate the adsorption of the compounds on particulate matter. The aqueous solution is representative of the water layer that is usually found on the particle surface.[29] To achieve deposition, each target quinone was dissolved in $CH_2Cl_2$ and the glass spheres were added. Dichloromethane was then evaporated using a Büchi 011 Rotavapor device equipped with a Büchi 461 heating bath. The quinone-loaded glass spheres (10% w/w) were stored under refrigeration and suspended in water before use. The sphere loading was adjusted so as to obtain an initial quinone concentration of 1 mM in the irradiated systems.

### Irradiation experiments

Irradiation was carried out in cylindrical Pyrex glass cells (4.0 cm diameter, 2.3 cm height, tightly closed with a lateral screw cap), containing 5 mL of aqueous phenol solution in which the glass spheres were dispersed. The suspensions were magnetically stirred during irradiation. The adopted light sources were: *(i)* a solar simulator (Solarbox, CO.FO.ME.GRA., Milan, Italy) equipped with a 1500 W Philips Xenon lamp and a 310 nm cut-off filter. The radiation intensity incident on the cells was 25 W $m^{-2}$, measured with a CO.FO.ME.GRA. power meter in the wavelength interval of 290-400 nm; *(ii)* a 40 Watt Philips TL K03 lamp with emission maximum at 435 nm (blue light). The total incident photon flux in the cells was $Q_o = 1.8 \times 10^{-5}$ einstein $L^{-1}$ $s^{-1}$, actinometrically determined using the ferrioxalate method.[30] The calculations to obtain $Q_o$ have taken into account the lamp spectrum, the radiation absorption of 0.15 M ferrioxalate and its photolysis quantum yield.[31] Figure 1 reports the emission spectrum of the blue lamp (spectral photon flux density, $q°_{n,p}(\lambda)$), measured with an Ocean Optics SD2000 CCD spectrophotometer and normalised to the actinometry data.

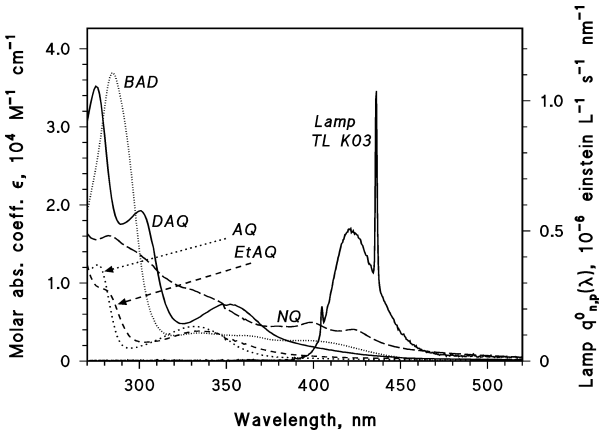


**Figure 1.** Spectral photon flux $q^0_{n,p}(\lambda)$ of the Philips TL K03 lamp. Molar absorption coefficients $\varepsilon(\lambda)$ of the quinones under study, taken in a 90:10 $H_2O$:$CH_3CN$ mixture.

In the irradiation experiments under $N_2$ atmosphere, air was eliminated from the cells by bubbling into the suspension a gentle flow of high-purity $N_2$ (99.998%, SIAD, Bergamo, Italy), for 20 min prior to irradiation.

Figure 1 also reports the absorption spectra of the quinones under study (molar absorption coefficients $\varepsilon(\lambda)$), taken in 90:10 water:acetonitrile with a Varian Cary 100 Scan UV-Vis spectrophotometer. The absorbed photon flux $P_a$ (einstein $L^{-1}$ $s^{-1}$) of the studied quinones under the blue lamp can be approximately derived as the integral over wavelength of the product between the spectral photon flux of the lamp and the fraction of light absorbed by each compound (absorption factor $f(\lambda)$).[32] It is $f(\lambda) = 1 - 10^{-\varepsilon(\lambda)\, b\, c}$, where $c$ is the quinone concentration (1 mM) and $b$ the optical path length of the solution (0.4 cm).

$$P_a = \int_{\lambda} q^0_{n,p}(\lambda) \cdot \left(1 - 10^{-\varepsilon(\lambda)\cdot b\cdot c}\right) d\lambda \qquad (8)$$

The described approach is approximated for a number of reasons: *(i)* the spectra (Figure 1) have been recorded in 90:10 water:acetonitrile, while the quinones have been deposited in the solid form on the glass spheres and irradiated in the presence of water. Some solvatochromic effects can be expected and the actual absorption spectra in the irradiated systems could be slightly different; *(ii)* the Lambert-Beer approach of equation (8) is not an exact representation of the irradiated systems, which were heterogeneous because the quinones were present in the solid form over the glass spheres.

### Sample treatment after irradiation

It was necessary to characterise both the dissolved compounds and those present on the glass spheres. After irradiation, 4 mL of the quinone suspension were filtered on Millipore Millex HV syringe filters. The filtered aqueous phase was divided into two parts: one was directly analysed by liquid chromatography (HPLC-UV, quantification of phenol), the other underwent solvent extraction with $CH_2Cl_2$ followed by analysis in gas-chromatography coupled with mass spectrometry (GC-MS) to characterise the water-dissolved transformation intermediates. Prior to solvent extraction, the aqueous phase was acidified with 0.9 M $H_2SO_4$ and salted with $Na_2SO_4$. Each sample was extracted three times with 1 mL $CH_2Cl_2$ each, and the three extracts were put together. Water traces were eliminated with anhydrous $Na_2SO_4$, the extract was concentrated under a gentle flow of high-purity nitrogen and analysed by Gas Chromatography – Mass Spectrometry (GC-MS).

The quinone-coated glass spheres remaining on the HV filter were extracted twice with 1 mL $CH_2Cl_2$ each, and the two extracts were put together. Water traces were eliminated with $Na_2SO_4$ and the extracts analysed by GC-MS. Evaporative concentration of the extract was not carried out at this stage, aimed at quinone quantification.

Some dedicated irradiation experiments were carried out for the identification of the transformation intermediates present on the glass spheres. In this case the suspension after irradiation was filtered on HV membranes, each filter extracted three times with 1 mL $CH_2Cl_2$ each, and the extracts put together. It followed water elimination with $Na_2SO_4$, concentration under a gentle $N_2$ flow, and analysis by GC-MS.

### GC-MS analysis

The dichloromethane extracts were analysed with a Finnigan Thermoquest Trace GC Series connected to an ion trap GCQ Plus mass analyser. The instrument was equipped with a phenyl-methylsilicone capillary column (HP 5 MS, 30 m length, 0.25 mm ID, 0.25 μm film thickness). Conditions employed were: carried flow (He) 1 mL $min^{-1}$, splitless injection (1 μL) for 30 s, injector temperature 300 °C, oven temperature 40°C (3 min), then to 300°C at 15°C $min^{-1}$, and stay at 300°C for 10 min. Quantification was carried out with the external standard method. In the irradiated systems containing phenol and EtAQ it was possible to identify the following transformation intermediates (retention times are in brackets, structures are reported in Scheme ESI2): 2-phenoxyphenol (12.85), 2,2'-dihydroxybiphenyl (13.76), 4-phenoxyphenol (14.24), 2,4'-dihydroxybiphenyl (15.18), 9,10-anthraquinone (16.06), 4,4'-dihydroxybiphenyl (16.54), 2-(1-hydroxyethyl)anthraquinone (18.05) and 2-(1-oxoethyl)anthraquinone (18.42). The retention times of phenol and EtAQ were 7.08 and 17.49 min, respectively.

### HPLC-UV analysis

The time evolution of phenol present in the dissolved phase was monitored by HPLC-UV, using a Merck-Hitachi chromatograph equipped with a RP-C18 LichroCART column (Merck, length 125 mm, diameter 4 mm) packed with LiChrospher 100 RP-18 (5 μm diameter). The samples were isocratically eluted with a 50:50 mixture of acetonitrile: water (1.0 mL $min^{-1}$ flow rate), and detected at 210 nm. Under these conditions the column dead time was 0.90 min. The retention times of the different compounds were (min): phenol (2.25), 4-nitrophenol (2.95), 2-nitrophenol (4.20), and 2-EtAQ (6.65).

### $H_2O_2$ determination

The analysis of hydrogen peroxide in the aqueous phase after filtration was carried out in dedicated experiments with horseradish peroxidase.[33] The adopted procedure was as follows: 1 mg enzyme was dissolved in 100 mL aqueous solution containing 25 mM phenol, 4.9 mM 4-aminoantipyrine, 1.0 mM phosphate buffer (pH 6.9), and 2.5 μM $H_2O_2$ to preserve the enzyme, but with negligible effects on the detection limit of the method. Aliquots of the solutions after irradiation (0.3 mL) were added to 2 mL enzyme solution and diluted with water to 5 mL. The absorbance was spectrophotometrically measured at 505 nm. The detection limit of $H_2O_2$ was around 3 μM.

### Quantum mechanical calculations

A study of the excited-state properties of AQ, DAQ and EtAQ was carried out by employing the density functional theory (DFT). DFT techniques have already been used to predict the absorption spectra of AQ and related compounds.[34,35] The present work aims at exploring the features of the triplet states of AQ, DAQ and EtAQ, with particular interest into the spin density distribution over the molecular orbitals and the geometry of the molecules in the excited state.

Geometry optimisations in ground state ($S_0$) of AQ, DAQ and EtAQ were carried out in the gas phase and were confirmed by analytical calculation of frequencies. An optimisation of the lowest-lying triplet state ($T_1$) was also performed. For each molecular species, the gas-phase optimised structures were determined by gradient procedures, within the Density Functional Theory (DFT) and the B3LYP hybrid functional.[36] The latter is a well-performing functional for polycyclic aromatic systems and their functionalised derivatives such as the anthraquinones.[37] The polarised 6-311G(d,p) basis set was used in all the calculations, and the nature of the stationary points was confirmed by analytical calculation of the vibrational frequencies. All calculations were carried out with the GAUSSIAN 03W suite of programs.[38] The figures were generated with the GaussView program.

## Results and discussion

Figure 2 reports the time evolution of 20 μM phenol upon irradiation under simulated sunlight, in the presence of the glass spheres alone or the different quinones supported on the spheres (1 mM quinone concentration in each 5-mL system). It is apparent that all the quinones enhanced phenol degradation compared to the naked glass spheres. The reactivity order was EtAQ > BAD > AQ ≈ NQ > DAQ. The most reactive quinone under simulated sunlight (EtAQ) was selected for the study of the reaction pathways.

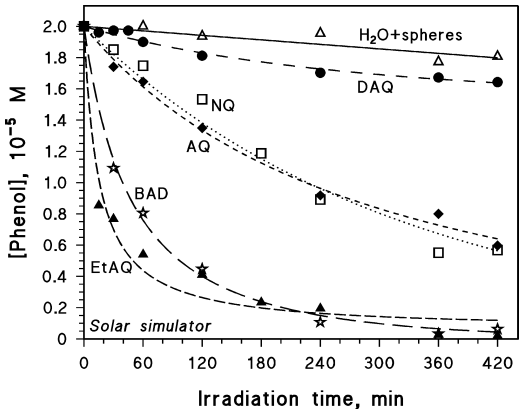


**Figure 2.** Time evolution of phenol (initial concentration 20 μM) in the presence of the glass spheres alone or the quinones (1 mM total concentration) supported on the spheres. Irradiation under simulated sunlight.

### Irradiation of phenol and EtAQ

Within the studied systems, EtAQ was detected both in the aqueous phase and on the spheres, but its amount was considerably higher on the latter. The concentrations of EtAQ in the two phases were summed up and the total one is here reported. Phenol was exclusively present in solution.

Figure 3 shows the time evolution of 0.1 mM phenol and 1 mM EtAQ upon irradiation under simulated sunlight, in aerated solution and under $N_2$ atmosphere. Insignificant phenol transformation was observed upon irradiation in the presence of the glass spheres only, without EtAQ. In this way it is possible to exclude the direct photolysis of phenol or a significant photoactivity of the glass spheres under the adopted conditions. EtAQ in aerated solution was able to photosensitise the degradation of phenol, and to undergo degradation as well. Both phenol and EtAQ underwent faster degradation in aerated solution than under $N_2$ atmosphere.

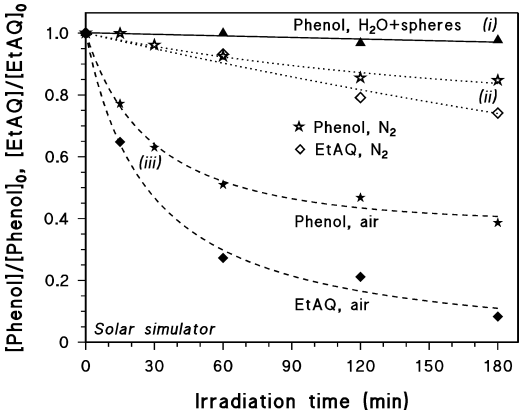


**Figure 3.** Time evolution of *(i)* 0.1 mM phenol in the presence of the glass spheres, not loaded with EtAQ. *(ii)* 0.1 mM phenol + 1 mM EtAQ loaded on the glass spheres, under $N_2$ atmosphere. *(iii)* 0.1 mM phenol + 1 mM EtAQ loaded on the glass spheres, in aerated solution. Irradiation under simulated sunlight.

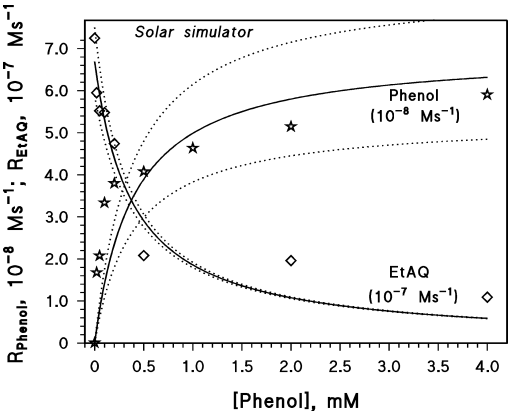


**Figure 4.** Initial transformation rates of phenol and of 1 mM EtAQ in aerated solution as a function of phenol initial concentration. Irradiation under simulated sunlight. Data fit with equations (19,20). The dotted curves represent the 95% confidence bands of the fit.

Figure 4 reports the initial transformation rates of phenol ($R_{Phenol}$) and of 1 mM EtAQ ($R_{EtAQ}$), calculated from the initial slope of the time evolution curves, as a function of phenol concentration. Note the different scales of the plot in Figure 4: the degradation rates of phenol (around $10^{-8}$ M $s^{-1}$) were considerably lower than those of EtAQ (about $10^{-7}$ M $s^{-1}$). Interestingly, the degradation rates of EtAQ and phenol show opposite trends with phenol concentration. Such a behaviour suggests that the two compounds could compete for the same reactive species. In the case of the quinones, this is usually the excited triplet state.[17,18,39] It can thus be hypothesised that $EtAQ^{T1}$ reacts with both ground-state EtAQ and phenol.

GC-MS analysis enabled the identification of the following transformation intermediates of EtAQ: 2-(1-oxoethyl)anthraquinone (main intermediate), 2-(1-hydroxyethyl)anthraquinone, and 9,10-anthraquinone (see Scheme ESI2 for the structures). All the compounds were detected in the aqueous phase, and 2-(1-hydroxyethyl)anthraquinone also on the glass spheres. Trace amounts of a compound that could be the hydroquinone derivative of EtAQ (2-ethyl-9,10-dihydroxyanthracene) were also detected on the glass spheres. The detected intermediates suggest that the main oxidation pathway of EtAQ would involve the alkyl lateral chain. This datum is compatible with a reaction where $EtAQ^{T1}$ extracts an hydrogen atom from EtAQ, a very common reaction pathway for light-excited quinones.[19] Moreover, the reduction of $EtAQ^{T1}$ by EtAQ would yield the semiquinone radical EtAQ-H$^{\bullet}$. The latter could yield the corresponding hydroquinone by further reduction. Interestingly, the hydroquinone was tentatively detected only at trace levels by GC-MS. In aerated solution the most likely explanation is that EtAQ-H$^{\bullet}$ reacts promptly with dissolved $O_2$ to give EtAQ and $HO_2^{\bullet}$. In the absence of oxygen, EtAQ-H$^{\bullet}$ could react with oxidised EtAQ or oxidised phenol to yield the initial substrates. The result would be a null cycle that would slow down the transformation kinetics, coherently with the experimental data obtained under $N_2$

atmosphere. A similar scenario has already been observed in the case of anthraquinone-2-sulphonate, AQ2S.[23]

GC-MS analysis of the aqueous phase yielded 2,2'-, 2,4'- and 4,4'-dihydroxybiphenyl and 2- and 4-phenoxyphenol as transformation intermediates of phenol (see Scheme ESI2 for the structures). These compounds can be formed upon reaction between phenol and the phenoxyl radical,[40] which suggests the formation of phenoxyl upon phenol oxidation by $EtAQ^{T1}$.

Catechol, hydroquinone and 1,4-benzoquinone were not detected as phenol transformation intermediates, by either GC or HPLC. All these compounds are formed by phenol and $^{\bullet}OH$,[41] and 1,4-benzoquinone also by phenol and $^1O_2$.[42] In analogy with previous results obtained with AQ2S,[23] one can exclude an important role of either $^{\bullet}OH$ or $^1O_2$ in the transformation of phenol or EtAQ.

It is possible to propose a kinetic model to describe the transformation of EtAQ and phenol. The model involves irradiation of EtAQ (with absorbed photon flux $P_a$) to yield the excited singlet state $EtAQ^{S1}$. It follows either deactivation, or inter-system crossing (ISC) to give $EtAQ^{T1}$ with quantum yield $\Phi$ (reaction 9). The triplet state could undergo deactivation (reaction 10) or oxidise the ground states of both phenol and EtAQ (reactions 11, 12). The radical intermediates are indicated as $EtAQ_{red}$, $EtAQ_{ox}$ and $Phen_{ox}$. $EtAQ_{red}$ could react with oxygen (reaction 15), $EtAQ_{ox}$ (reaction 13), or $Phen_{ox}$ (reaction 14). Reaction of $EtAQ_{red}$ with $EtAQ_{ox}$ or $Phen_{ox}$ would give back the initial substrates and account for the low reaction rates observed under $N_2$ atmosphere. Reaction (15) between $EtAQ_{red}$ and $O_2$ would yield EtAQ and $HO_2^{\bullet}/O_2^{-\bullet}$ (reaction 16).

$$EtAQ \xrightarrow{h\nu} EtAQ^{S1} \xrightarrow{ISC} EtAQ^{T1} \quad (9)$$

$$EtAQ^{T1} \xrightarrow{k_{10}} EtAQ \quad (10)$$

$$EtAQ^{T1} + Phenol \xrightarrow{k_{11}} EtAQ_{red} + Phen_{ox} \quad (11)$$

$$EtAQ^{T1} + EtAQ \xrightarrow{k_{12}} EtAQ_{red} + EtAQ_{ox} \quad (12)$$

$$EtAQ_{red} + EtAQ_{ox} \xrightarrow{k_{13}} 2\ EtAQ \quad (13)$$

$$EtAQ_{red} + Phen_{ox} \xrightarrow{k_{14}} EtAQ + Phenol \quad (14)$$

$$EtAQ_{red} + O_2 \xrightarrow{k_{15}} (EtAQ_{red}O_2) \quad (15)$$

$$(EtAQ_{red}O_2) \xrightarrow{k_{16}} EtAQ + HO_2^{\bullet}/O_2^{-\bullet} \quad (16)$$

$$Phen_{ox} \xrightarrow{k_{17}} Products_{\ Phen} \quad (17)$$

$$EtAQ_{ox} \xrightarrow{k_{18}} Products_{\ EtAQ} \quad (18)$$

In the absence of $O_2$ the reactions (9-14) would constitute a null cycle with negligible transformation of the substrates. The fact that, under $N_2$ atmosphere, the transformation of EtAQ and phenol was slow but not nil (Figure 3) suggests that reactions (17,18) would not be completely negligible compared to (13,14) when oxygen is not available. Manageable solutions of the kinetic system can be obtained for aerated media under the hypothesis that reactions (13,14) are negligible compared to (15), and by application of the steady-state approximation to $EtAQ^{T1}$, $EtAQ_{red}$, $(EtAQ_{red}O_2)$, $EtAQ_{ox}$, and $Phen_{ox}$. Under this hypothesis one gets the following expressions for the initial transformation rates of EtAQ and phenol ($R_{EtAQ}$ and $R_{Phenol}$, respectively):

$$R_{EtAQ} = \frac{a \cdot k_{12} \cdot k_{11}^{-1} \cdot [EtAQ(t)]}{b + [Phenol(t)]} \quad (19)$$

$$R_{Phenol} = \frac{a \cdot [Phenol(t)]}{b + [Phenol(t)]} \quad (20)$$

where $a = \Phi\ P_a$ and $b = k_{11}^{-1}\ (k_{10} + k_{12}\ [EtAQ(t)])$. The fit of the initial rate data ($t$ = 0) of EtAQ and phenol with equations (19,20) is reported in Figure 4, with reasonable agreement considering the heterogeneous nature of the studied systems. The fit yielded $a = (6.95 \pm 1.86) \cdot 10^{-8}$, $k_{12}\ k_{11}^{-1} = 3.7 \pm 1.0$ and $b = (3.9 \pm 1.1) \cdot 10^{-4}$ (error bounds represent $\pm\sigma$).

Finally, the formation of $HO_2^{\bullet}/O_2^{-\bullet}$ in reaction (16) would be followed by disproportionation and production of $H_2O_2$.[23] Indeed, around 0.1 mM $H_2O_2$ was formed upon 3-h irradiation of 20 μM phenol and 1 mM sphere-supported EtAQ under simulated sunlight.

**Quantum yields of phenol phototransformation under blue light**

Irradiation under the blue lamp (Philips TL K03) was carried out to enable an (approximate) assessment of the photon flux absorbed by the quinones and, as a consequence, of the quantum yields of phenol phototransformation. Figure 5 reports the time trend of 20 μM phenol with the different quinones. In all the cases the sphere-supported quinones enhanced phenol transformation compared to the naked glass spheres, and the reactivity order was similar to that observed with the solar simulator (Figure 2). A notable exception is EtAQ, which showed limited reactivity under blue light. The most likely reason is that EtAQ has an absorption maximum around 340 nm and absorbs only a limited fraction of the radiation emitted by the blue lamp (see Figure 1).

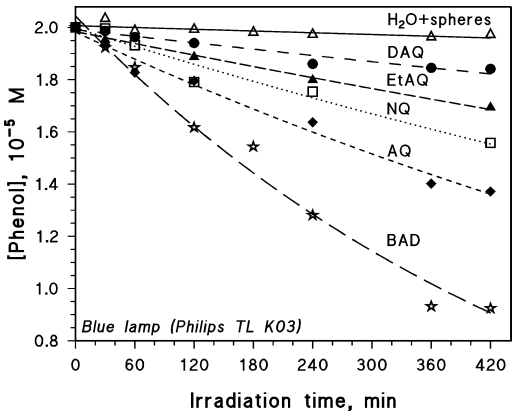


**Figure 5.** Time evolution of phenol (initial concentration 20 μM) in the presence of the glass spheres alone or the quinones (1 mM total concentration) supported on the spheres, under blue light (Philips TL K03 lamp). Note the zoomed Y-axis, which starts from 0.8.

Table 1 reports the photon fluxes absorbed by the different quinones ($P_a$, calculated by equation 8), the initial rates of phenol transformation ($R_P$) and the (approximate) polychromatic photodegradation quantum yields ($\Phi = R_P\ P_a^{-1}$). The latter were in the order AQ > BAD > EtAQ > NQ > DAQ.

**Table 1.** For each studied quinone it is reported: *(i)* the (approximate) absorbed photon flux ($P_a$) under the adopted irradiation conditions, calculated with equation (8) under the Lambert-Beer approximation and upon numerical integration; *(ii)* the initial degradation rate of phenol ($R_P$) upon quinone irradiation under blue light, calculated as the initial slope of the time evolution curves of phenol in Figure 5; *(iii)* the polychromatic quantum yield of phenol photodegradation, $\Phi = R_P\, P_a^{-1}$.

| Quinone | $P_a$, einstein $L^{-1}$ $s^{-1}$ | $R_P$, M $s^{-1}$ | $\Phi$ |
|---|---|---|---|
| NQ | $1.6\cdot10^{-5}$ | $2.1\cdot10^{-10}$ | $1.3\cdot10^{-5}$ |
| DAQ | $9.6\cdot10^{-6}$ | $7.0\cdot10^{-11}$ | $7.3\cdot10^{-6}$ |
| EtAQ | $5.6\cdot10^{-6}$ | $1.3\cdot10^{-10}$ | $2.3\cdot10^{-5}$ |
| BAD | $1.2\cdot10^{-5}$ | $6.4\cdot10^{-10}$ | $5.3\cdot10^{-5}$ |
| AQ | $3.6\cdot10^{-6}$ | $3.0\cdot10^{-10}$ | $8.3\cdot10^{-5}$ |

To get further insight into the different reactivity of the studied compounds, a DFT quantum mechanical study was carried out of the ground ($S_0$) and excited triplet states ($T_1$) of the quinones that showed the highest (AQ) and the lowest (DAQ) quantum yield for phenol degradation. The geometry optimisation of the structures is reported in ESI. To understand the nature of the excited state, a total spin density surface of AQ $T_1$ has been created and is reported in Figure 6a. There are two main areas where the spin density is the highest: the strongest one is centred on the carbonyl group, the other one is on the atoms that allow the resonance of unpaired electrons over the aromatic skeleton of the molecule. In particular, the spin density distribution of the carbonyl group that is more involved in the $S_0 - T_1$ transition (and that undergoes the highest bond lengthening, see ESI for details) is localised on the π* system, unoccupied in the $S_0$ state. This is in reasonable analogy with the distribution shown by the CO molecule in its lower-lying triplet state (Figure 6b).

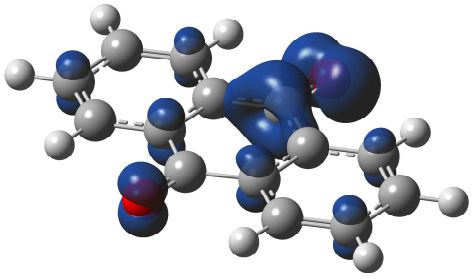

a) AQ

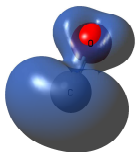

b) CO

**Figure 6. a)** Spin density surface of AQ in its $T_1$ state (isovalue = 0.005) at right angled view (faded). **b)** Spin density surface (faded) of CO in its $T_1$ state (isovalue = 0.01).

In contrast, the spin density present on the oxygen atom of the other carbonyl group is itself the result of resonance on the AQ skeleton. The reason is the favourable position of the oxygen *p* orbital that is parallel to the aromatic π system. Hydrogen atoms exhibit negligible spin density. Considering that the photochemical processes involving $AQ^{T1}$ would probably lead to its reduction to a semiquinone radical species (in analogy with EtAQ, see reactions 9-18), one can expect that the spin density on the carbonylic oxygen is connected with the photochemical reactivity of AQ. In contrast, the spin density delocalised over the aromatic skeleton would not be linked with reactivity, because the addition of an electron or a hydrogen atom there would destabilise the aromaticity of the molecule and generate unstable photoproducts.

If the assumption reported above is correct, one should expect to find a similar spin distribution also in the case of $EtAQ^{T1}$, which is expected to oxidise phenol and undergo reduction to a semiquinone radical. Figure 7 reports the spin density surface of the EtAQ molecule in its $T_1$ state. It is very similar to that observed for AQ. Also in this case there are two main areas where the spin density is concentrated: the main one is centred on the carbonyl group, the other over the aromatic skeleton of the molecule. When considering the DFT results and the likely reactivity of EtAQ, there appears to be a link between spin distribution on the carbonyl group and the ability of that group to be involved in redox reactions.

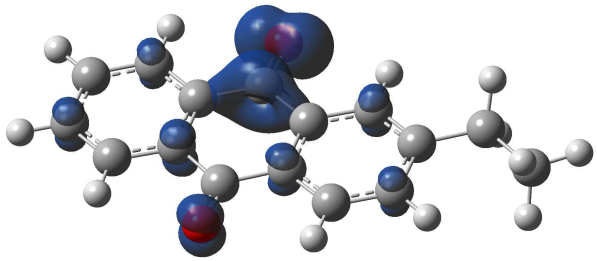

**Figure 7**. Spin density surface of EtAQ in its $T_1$ state (isovalue = 0.005) at right angled view (faded).

For the DAQ molecule in its $T_1$ state, the interpretation of the spin density surface reported in Figure 8 is more complex. The molecule has two -OH substituents, which leads to a change in symmetry from $D_{2h}$ of AQ to $C_{2h}$ of DAQ (EtAQ has $C_S$ symmetry). Interestingly and differently from AQ, the spin distribution over the most elongated carbonyl group does not show the carbon monoxide-like pattern over the π* system. In contrast, a significant fraction of the spin density is delocalised on one of the lateral aromatic rings that bear the OH substituents. Interestingly, the conjugation between the OH group and the dienic portion of the ring causes the ring itself to evolve from a phenolic-type into a quinoid-type structure, with consequent readjustment of the bond lengths (see ESI for the details of geometry optimisation). Figure 9 gives a pictorial scheme of the cited effects, highlighting the changes in bond features that occur from $S_0$ to $T_1$.

Adiabatic and vertical transition energies for AQ, EtAQ and DAQ are reported in Table ESI9.

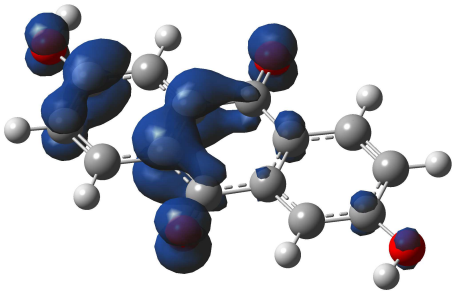

**Figure 8**. Spin density surface of DAQ in its $T_1$ state (isovalue = 0.005) at right angled view (faded).

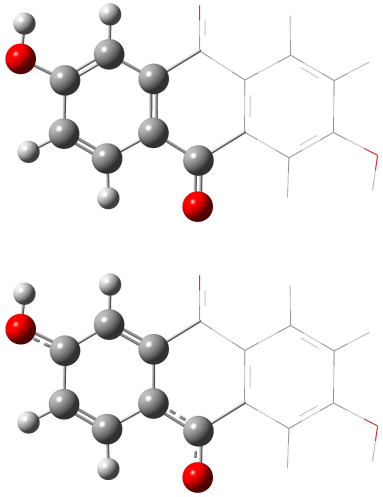

**Figure 9.** Molecular structures of DAQ showing through bond type the transition effects from $S_0$ (above) to $T_1$ (below) states, to underline the change in bond types. The molecular portion remarkably involved in spin resonance is highlighted through balls and stick representation, while the rest of the molecule is depicted through wireframe.

Table 2 reports spin density values, expressed as percentage, for some molecular regions that could be meaningful for anthraquinone photochemistry. Looking at the values reported in the table, it can be observed that the spin density of AQ is mainly located on the carbonylic oxygen (57 %), while the remaining is spread over the carbon skeleton of the molecule. This means that a substantial part of the unpaired electrons is placed on the photoreactive carbonyl group, which could justify the high reactivity of AQ in terms of quantum yield of phenol transformation. The spin distribution of EtAQ is practically equal to that of AQ, because the ethyl group appears not to affect the spin resonance over the anthraquinone skeleton of the molecule. In contrast, in the case of DAQ most of the spin density (65 %) is distributed on the carbon skeleton that would not be involved into photochemical reactions. Only 27 % of the DAQ $T_1$ spin density is located on the carbonylic oxygen, which would result into lower photoactivity compared to AQ.

**Table 2.** Spin density distribution over AQ, EtAQ and DAQ molecules, expressed in terms of percentage (the sum of Mulliken atomic spin density is 2.00). n/a = not applicable.

| | AQ (%) | EtAQ (%) | DAQ (%) |
|---|---|---|---|
| | 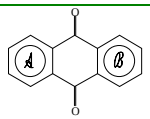 | 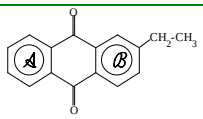 | 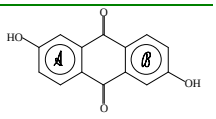 |
| Ring A | 14 | 14 | 55 |
| Ring B | 14 | 13 | 10 |
| O of C=O | 57 | 57 | 27 |
| C of C=O | 15 | 16 | 0 |
| O of OH | n/a | n/a | 8 |

**Phenol photonitration upon irradiation of the studied quinones and nitrite**

Figure 10 reports the time evolution of 2-nitrophenol (2NP) and 4-nitrophenol (4NP) upon irradiation of 1 mM phenol and 0.10 M nitrite under the blue lamp. Irradiation was carried out with nitrite alone and in the presence of the quinones supported on the glass spheres (1 mM total quinone loading in all the cases). The most reactive quinones under blue light (AQ, BAD and NQ) were selected for this study. It can be observed that all the adopted quinones enhanced the formation of 2NP and 4NP compared to nitrite alone. The reactivity order was NQ > BAD > AQ.

The photonitration of phenol is accounted for by reaction with $^{\bullet}NO_2$.[43] In the presence of nitrite alone, nitrogen dioxide is formed upon oxidation of $NO_2^-$ by the photogenerated $^{\bullet}OH$ radicals (reactions 21,22):[44]

$$NO_2^- + h\nu + H^+ \rightarrow {}^{\bullet}OH + {}^{\bullet}NO \qquad (21)$$

$$NO_2^- + {}^{\bullet}OH \rightarrow {}^{\bullet}NO_2 + OH^- \qquad (22)$$

Phenol photonitration in neutral solution is a useful probe of $^{\bullet}NO_2$,[45] thus the enhancement of nitrophenol formation by irradiated quinones suggests a higher availability of nitrogen dioxide. It can be hypothesised that the adopted quinones are able to oxidise nitrite under photochemical conditions, according to the following process (Q = quinone):

$$Q + h\nu \rightarrow Q^{S1} \text{—(ISC)}\rightarrow Q^{T1} \qquad (23)$$

$$Q^{T1} + NO_2^- \rightarrow Q^{-\bullet} + {}^{\bullet}NO_2 \qquad (24)$$

Interestingly, the production of nitrogen dioxide by nitrate photolysis and by nitrite oxidation by $^{\bullet}OH$ is an important $^{\bullet}NO_2$ source in atmospheric waters, possibly prevailing over dissolution of $^{\bullet}NO_2$ from the gas phase.[46] Moreover, nitrite photochemistry is a major source of radical species in irradiated fog and rain water.[47,48] The results reported here suggest that the oxidation of nitrite by light-excited quinones might play a role as a source of $^{\bullet}NO_2$ and nitroaromatic compounds on the particle surface. Similarly, it has been shown that nitrite oxidation by photoexcited chromophoric dissolved organic matter can be a significant $^{\bullet}NO_2$ source in organic-rich surface waters, and that quinoid compounds are probably involved in the process.[45]

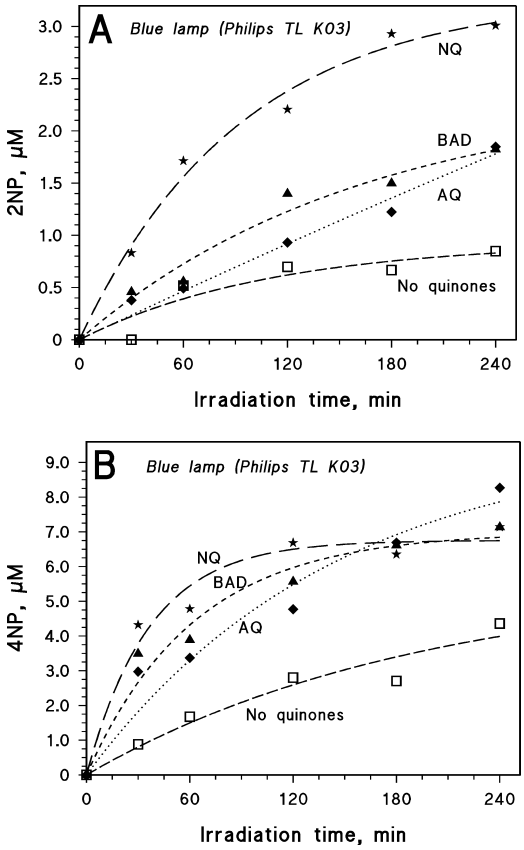


**Figure 10. (A)** Time evolution of 2-nitrophenol (2NP) upon irradiation of 1 mM phenol + 0.10 M $NaNO_2$, alone or in the presence of the quinones supported on the glass spheres (1 mM total quinone loading). Irradiation under the Philips TL K03 lamp (blue light). **(B)** Time evolution of 4-nitrophenol (4NP) under the same conditions as above.

## Conclusions

This work shows that quinones supported on glass spheres are able to sensitise the transformation of phenol in irradiated aqueous solution. Such a process is relevant to the photochemistry of quinones present on airborne particles, the surface of which is usually covered by a water layer.[29] Among the studied photosensitisers, the order of the quantum yields for phenol phototransformation under blue light was AQ > BAD > EtAQ > NQ > DAQ. For AQ and DAQ, DFT calculations showed very different spin density distributions in the $T_1$ state. In the case of AQ (and of EtAQ), most of the spin density is centred over the oxygen atom of the carbonyl group, which is reasonable considering that $AQ^{T1}$ would oxidise phenol and undergo reduction to a semiquinone radical. In the case of DAQ most of the spin density is delocalised over the unreactive aromatic skeleton, which could account for the lower photoactivity.

EtAQ was the most reactive quinone toward phenol transformation under simulated sunlight. The investigation of phenol transformation by EtAQ supported on glass spheres led to a kinetic model made up of reactions (9-18), able to account for the experimental data. According to the model, radiation-excited EtAQ ($EtAQ^{T1}$) would oxidise the ground states of both EtAQ and phenol. In aerated solution the oxidised radicals would evolve into lateral-chain oxidation compounds (from EtAQ), dihydroxybiphenyls and phenoxyphenols (from phenol). $EtAQ^{T1}$ would undergo reduction, and in aerated solution the reduced radical (most likely a semiquinone) would react with $O_2$ to yield back EtAQ. In the absence of oxygen, reduced and oxidised species would generate back the starting compounds, in a null cycle that would keep the reaction rates very low.

Phenol transformation intermediates are compatible with the formation of phenoxyl radical in the primary reaction step(s), and it is also suggested that environmentally concerning secondary pollutants can be formed in the presence of phenolic compounds and quinones under irradiation. Phenol intermediates are also not compatible with the occurrence of reactive species such as $^{\bullet}OH$ or $^1O_2$. Furthermore, dihydroxybiphenyls and phenoxyphenols can potentially be the first steps of an oligomerisation process, similar to the reactions that yield the humic-like substances in the atmosphere.[49,50]

Photoexcited quinones can oxidise nitrite to nitrogen dioxide, which enhances phenol nitration compared to the irradiation of nitrite alone. Such a process could lead to significant generation of phytotoxic nitrophenols in the atmospheric aqueous phase, which could contribute to vegetation damage. Because of the potential importance of quinone-enhanced nitration, further investigation will be required to assess its significance in the atmospheric aerosol phase.

## Acknowledgements

Financial support from PNRA-Progetto Antartide is gratefully acknowledged. We are thankful to Prof. Eliano Diana for useful discussion.

## Notes and references

[a] *Dipartimento di Chimica Analitica, Università di Torino, Via P. Giuria 5, 10125 Torino, Italy.* http://www.chimicadellambiente.unito.it. *Fax: +39-011-6707615;E-mail:* claudio.minero@unito.it davide.vione@unito.it

[b] *Centro Interdipartimentale NatRisk, Università di Torino, Via Leonardo Da Vinci 44, 10095 Grugliasco (TO), Italy.* http://www.natrisk.org

† Electronic Supplementary Information (ESI) available: quinone levels on airborne particulate, structure of the studied compounds and of the detected intermediates, optimised structures of AQ and DAQ. See DOI:10.1039/b000000x/

1 A. Jammoul, S. Gligorovski, C. George and B. D'Anna, *J. Phys. Chem. A*, 2008, **112**, 1268-1276.

2 S. Net, S. Gligorovski, S. Pietri and H. Wortham, *Phys. Chem. Chem. Phys.*, 2010, **12**, 7603-7611.

3 I. Grgic, L. I. Nieto-Gligorovski, S. Net, B. Temime-Roussel, S. Gligorovski and H. Wortham, *Phys. Chem. Chem. Phys.*, 2010, **12**, 698-707.

4 D. Vione, V. Maurino, C. Minero, E. Pelizzetti, M. A. J. Harrison, R. I. Olariu and C. Arsene, *Chem. Soc. Rev.*, 2006, **35**, 441-453.

5 C. Anastasio, B. C. Faust and C. J. Rao, *Environ. Sci. Technol.*, 1997, **31**, 218-232.

6 S. Canonica, B. Hellrung, P. Muller and J. Wirz, *Environ. Sci. Technol.*, 2006, **40**, 6636-6641.

7 M. Jang and S. R. McDow, *Environ. Sci. Technol.*, 1995, **29**, 2654-2660.

8 M. Jang and S. R. McDow, *Environ. Sci. Technol.*, 1997, **31**, 1046-1053.

9 J. O. Allen, N. M. Dookeran, K. Taghizadeh, A. L. Lafleur, K. A. Smith and A. F. Sarofim, *Environ. Sci. Technol.*, 1997, **31**, 2064-2070.

10 C. Minero and V. Maurino, *Study of the space-time distribution of compounds dangerous for human health in high-traffic areas*, Technical report to the Province of Torino, Italy, 2000.

11 T. E. Jensen and R. A. Hites, *Anal. Chem.*, 1983, **55**, 594-599.

12 Y. A. Levendis, A. Atal and J. B. Carlson, *Environ. Sci. Technol.*, 1998, **32**, 3767-3777.

13 W. F. Rogge, L. M. Hildemann, M. A. Mazurek, G. R. Carr and B. R. T. Simoneit, *Environ. Sci. Technol.*, 1998, **32**, 13-22.

14 A. H. Neilson, *PAHs and related compounds*, Springer, Berlin, 1998.

15 T. Corrales, F. Catalina, C. Peinado and N. S. Allen, *J. Photochem. Photobiol. A: Chem.*, 2003, **159**, 103-114.

16 R. G. Brinson, S. C. Hubbard, D. R. Ziudema and P. B. Jones, *J. Photochem. Photobiol. A: Chem.*, 2005, **175**, 118-128.

17 T. Del Giacco, L. Latterini and F. Elisei, *Photochem. Photobiol. Sci.*, 2003, **2**, 681-687.

18 H. Gorner, *Photochem. Photobiol. Sci.*, 2006, **5**, 1052-1058.

19 S. Patai, *The chemistry of the quinoid compounds*, Wiley, NY, 1974.

20 H. Gorner, *Photochem. Photobiol. Sci.*, 2004, **3**, 933-938.

21 V. Latour, T. Pigot, M. Simon, H. Cardy and S. Lacombe, *Photochem. Photobiol. Sci.*, 2005, **4**, 221-229.

22 A. E. Alegría, A. Ferrer, G. Santiago, E. Sepúlveda and W. Flores, *J. Photochem. Photobiol. A: Chem.*, 1999, **127**, 57-65.

23 V. Maurino, D. Borghesi, D. Vione and C. Minero, *Photochem. Photobiol. Sci.*, 2008, **7**, 321-327.

24 R. Volkamer, B. Klotz, I. Barnes, T. Imamura, K. Wirtz, N. Washida, K. H. Becker and U. Platt, *Phys. Chem. Chem. Phys.*, 2002, **4**, 1598-1610.

25 M. A. J. Harrison, S. Barra, D. Borghesi, D. Vione, C. Arsene and R. I. Olariu, *Atmos. Environ.*, 2005, **39**, 231-248.

26 J. Lüttke, V. Schher, K. Levsen, G. Wöünsch, J N. Cape, K. J. Hargreaves, R. L. Storeton-West, K. Acker, W. Wieprecht and B. Jones, *Atmos. Environ.*, 1997, **31**, 2637-2648.

27 D. Vione, V. Maurino, C. Minero and E. Pelizzetti, *Environ. Sci. Technol.*, 2005, **39**, 7921-7931.

28 M. A. J. Harrison, M. R. Heal and J. N. Cape, *Atmos. Chem. Phys.*, 2005, **5**, 1679-1695.

29 V. Samburova, T. Didenko, E. Kunenkov, C. Emmenegger, R. Zenobi and M. Kalberer, *Atmos. Environ.*, 2007, **41**, 4703-4710.

30 H. J. Kuhn, S. E. Braslavsky and R. Schmidt, *Pure Appl. Chem.*, 2004, **76**, 2105-2146.

31 J. G. Calvert and J. N. Pitts, *Photochemistry*, Wiley, NY, 1966.

32 S. E. Braslavsky, *Pure Appl. Chem.*, 2007, **79**, 293-465.

33 X. Q. Yang and K. Ma, *Anal. Biochem.*, 2005, **344**, 130-134.

34 L. Shen, H.-F. Ji and H.-Y. Zhang, *J. Mol. Struc. – Teochem*, 2008, **851**, 220-224.

35 J. Preat, D. Jacquemin, J. Burton, D. P. Vercauteren and E. A. Perpète, *Dyes Pigments*, 2009, **81**, 97-102.

36 J. B. Foresman and Æ. Frisch, *Exploring Chemistry with Electronic Structure Methods*, Gaussian, Inc., Pittsburgh, PA, 1996, pp. 166-168.

37 D. Jacquemin, J. Preat, M. Charlot, V. Wathelet, J. M. Andre and E. A. Perpete, *J. Chem. Phys.*, 2004, **121**, 1736-1743.

38 M. J. Frisch, G. W. Trucks, H. B. Schlegel, G. E. Scuseria, M. A. Robb, J. R. Cheeseman, V. G. Zakrzewski, J. A. Montgomery Jr., R. E. Stratmann, J. C. Burant, S. Dapprich, J. M. Millam, A. D. Daniels, K. N. Kudin, M. C. Strain, O. Farkas, J. Tomasi, V. Barone, M. Cossi, R. Cammi, B. Mennucci, C. Pomelli, C. Adamo, S. Clifford, J. Ochterski, G. A. Petersson, P. Y. Ayala, Q. Cui, K. Morokuma, D. K. Malick, A. D. Rabuck, K. Raghavachari, J. B. Foresman, J. Cioslowski, J. V. Ortiz, B. B. Stefanov, G. Liu, A. Liashenko, P. Piskorz, I. Komaromi, R. Gomperts, R. L. Martin, D. J. Fox, T. Keith, M. A. Al-Laham, C. Y. Peng, A. Nanayakkara, C. Gonzalez, M. Challacombe, P. M. W. Gill, B. Johnson, W. Chen, M. W. Wong, J. L. Andres, M. Head-Gordon, E. S. Replogle and J. A. Pople, *Gaussian 03, revision B.05*, Gaussian, Inc., Pittsburgh, PA, 2003.

39 P. R. Maddigapu, A. Bedini, C. Minero, V. Maurino, D. Vione, M. Brigante, G. Mailhot and M. Sarakha, *Photochem. Photobiol. Sci.*, 2010, **9**, 323-330.

40 J. Platz, O. J. Nielsen, T. J. Wallington, J. C. Ball, M. D. Hurley, A. M. Straccia, W. F. Schneider and J. Sehested, *J. Phys. Chem. A*, 1998, **102**, 7964-7974.

41 F. Machado and P. Boule, *J. Photochem. Photobiol. A: Chem.*, 1995, **86**, 73-80.

42 M. Nowakowska and M. Kepczynski, *J. Photochem. Photobiol. A: Chem.*, 1998, 116, 251-256.

43 P. R. Maddigapu, D. Vione, B. Ravizzoli, C. Minero, V. Maurino, L. Comoretto and S. Chiron, *Environ. Sci. Pollut. Res.*, 2010, **17**, 1063-1069.

44 J. Mack and J. R. Bolton, *J. Photochem. Photobiol. A: Chem.*, 1999, **128**, 1-13.

45 P. R. Maddigapu, C. Minero, V. Maurino, D. Vione, M. Brigante and G. Mailhot, *Chemosphere*, 2010, **81**, 1401-1406.

46 C. Minero, V. Maurino, E. Pelizzetti and D. Vione, *Environ. Sci. Pollut. Res.*, 2007, **14**, 241-243.

47 C. Anastasio and K. G. McGregor, *Atmos. Environ.*, 2001, **35**, 1079-1089.

48 A. Albinet, C. Minero and D. Vione, *Sci. Total Environ.*, 2010, **408**, 3367-3373.

49 A. Hoffer, G. Kiss, M. Blazso and A. Gelencser, *Geophys. Res. Lett.*, 2004, **31**, L06115.

50 B. J. Holmes and G. A. Petrucci, *J. Atmos. Chem.*, 2007, **58**, 151-166.